Journal of Nano- and Electronic Physics
Vol. **15** No 1, 01020(6pp) (2023)

Журнал нано- та електронної фізики
Том **15** № 1, 01020(6cc) (2023)

Effect of Temperature on the Performance of CGS/CIGS Tandem Solar Cell

Mourad Elbar[1,*], Souad Tobbeche[1], Slimane Chala[1,2,†], Okba Saidani[1], Mohamed Nadjib Kateb[1], Mohamed Redha Serdouk[1]

[1] *Laboratory of Metallic and Semiconducting Materials, Mohamed Khider University, 07000 Biskra, Algeria*
[2] *Institute of Electrical and Electronic Engineering, M'Hamed Bougara University, 35000 Boumerdes, Algeria*

(Received 03 January 2023; revised manuscript received 16 February 2023; published online 24 February 2023)

The CGS and CIGS being promising materials for large scale photovoltaic applications, the effect of temperature on the electrical parameters of a CGS/CIGS tandem solar cell has been investigated in this work. The copper gallium diselenide (CGS) and copper indium gallium diselenide (CIGS) structures as top-cell and bottom-cell respectively, were numerically simulated under AM1.5G spectral illumination using the two-dimensional device simulator Silvaco-Atlas. The temperature dependency of the solar cell's characteristics was investigated in the temperature range from 300 to 400 K at intervals of 20 K. The simulation results show the density current (J_{sc}) slightly increases whereas the open-circuit voltage (V_{oc}) and fill factor (FF), conversion efficiency (η) decreases with the increase in temperature. The tandem cell operating temperature efficiency was found to be (– 0.34 %/K), which is slightly higher than that of CGS solar cell (– 0.29 %/K), but markedly better than that of CIGS solar cell (– 0.41 %/K).

Keywords: Numerical simulation, Silvaco-Atlas, Temperature, CGS/CIGS Tandem cell, Matching current.

DOI: 10.21272/jnep.15(1).01020 PACS numbers: 78.20.Bh, 73.40.Lq, 84.60.Jt

1. INTRODUCTION

Due to their many unique properties such as low-cost of fabrication, large bandgap, high transparency, excellent conductivity, thin film solar cells have been, widely, used in many photovoltaic and optoelectronic applications [1-11].

The concept of tandem solar cells are the devices with two or more absorber layers with different bandgaps to absorb the maximum wavelength of the solar spectrum [12]. Tandem solar cells are combined with a narrow-bandgap bottom cell to absorb long-wavelength photons and awide-bandgap top cell to absorb the short-wavelength photons of solar spectrum energy [13-15].Because of the series connection, the efficiency of the tandem solar cell is limited by the solar cell that issues the lower current. An equal current criterion, among the cells building the tandem, must be achieved; all the cells must have the same photocurrent (current matching) [3, 4, 7, 14].

The temperature of tandem cells increases when they are used in systems under concentration or in space applications. Their electrical properties are significantly impacted by this phenomenon, which also disrupts their operation.

The temperature affects the solar cells in different ways.Its well-known that the physics governing solar cells operations extremely temperature dependent. The materials parameters like the energy gap (E_g), mobilities (μ_n and μ_p), and carriers densities (N_c and N_v) are also temperature dependent. Furthermore, the Solar cell is an optoelectronic device that is not converted the absorbed energy to electricity is converted to heat and thus increases the temperature inside the cells non-uniformly much beyond the ambient temperature [16].

The performance of a solar cell is influenced by temperature since its performance parameters, viz. short circuit current density (J_{sc}), open circuit voltage (V_{oc}), fill factor (FF), and efficiency (η) are temperature dependent [17]. The temperature variation affects these parameters and, hence, the performance of solar cells [16, 18]. The diode parameters of solar cells, i.e., reverse saturation current density(J_o) and ideality factor (n) along with series resistance (R_s) and shunt resistance (R_{sh}) control the effect of temperature on V_{oc}, FF and η of the cell [17].

The temperature dependence of performance on solar cells based on different materials. which showed with increasing temperature, short circuit current density (J_{sc}) increases, and therefore, open circuit voltage (V_{oc}) decreases which decreases the fill factor and hence the efficiency of the solar cell gave by [19] has been studied in the temperature range of 300-400 K, and in the temperature range of 273-523 K [20], 273-373 K [21]. Under the current matching condition slightly affects the temperature coefficient of the tandem cell, the top limited cell has a lower temperature coefficient than the bottom-limited and current-matched cells [22, 23].

In this work, a numerical study using the two-dimensional device simulator Silvaco-Atlas [24-27], to investigate the temperature behavior of optimal structure CGS/CIGS tandem cells is presented. In this paper, we aim to study the temperature effect on the electrical parameters of the tandem solar cells (open-circuit voltage V_{oc}, short-circuit current density J_{sc}, fill factor FF and conversion efficiency η).

2. CGS/CIGS TANDEM SOLAR CELL STRUCTURE AND NUMERICAL SIMULATION

Higher efficiencies could be obtained by stacking together different absorbers with different band gaps to maximize the light absorption. The basic structure optimale of the CGS/CIGS tandem solar cell is shown in Fig. 1.

* m.elbar@univ-biskra.dz
† s.chala@univ-boumerdes.dz

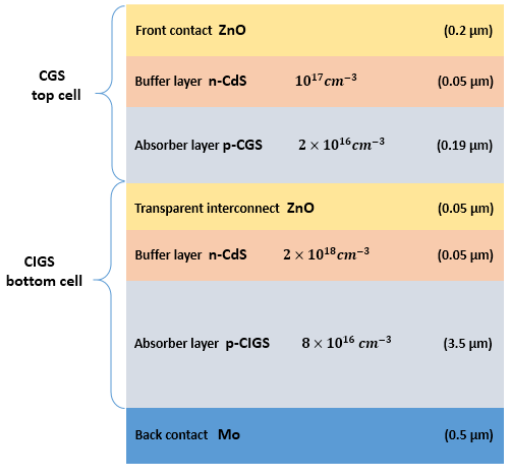

Fig. 1 – Tandem solar cell with CGS/CIGS subcells connected by transparent interconnect ZnO, the relative doping concentrations and the thicknesses are listed for each layer

It consisted of two solar cells where the CGS wide band-gap top cell had a small thickness and a large band gap ($E_g = 1.69$ eV) in contrast to the CIGS low band-gap bottom cell, which had a usual thickness for a CIGS cell and a band-gap value ($E_g = 1.16$ eV) close to the optimal values of best cells [28]. This design is intended to convert a wider range of photons incident on the solar cell therefore a maximum power output. The tandem cell consisted of a top n-CdS/p-CGS heterojunction and a bottom n-CdS/p-CIGS heterojunction. The top CGS and the bottom CIGS cells are optically and electrically connected with a transparent conducting oxide layer (TCO) of ZnO. The tandem solar cell was considered illuminated under AM 1.5 solar spectrum with 100 mW·cm^{-2} incident power density which was assumed to be normally incident on the top ZnO layer used as the cathode contact to the bottom metallic Molybdenum (Mo) forming the back anode contact of the tandem solar cell. The acceptor concentration in CIGS is generally around 2×10^{16} cm^{-3} [29], and we chosed $2 \times 10^{16}/8 \times 10^{16}$ cm^{-3} for CGS/CIGS in this study. The doping concentrations of donors and acceptors and thicknesses of the layers used in the simulation are indicated in Fig. 1.

3. SIMULATION PARAMETERS

The 2D Silvaco Atlas simulator requires input of the device parameters related to each layer and material in the cell structure. The semiconductor properties of ZnO, CdS, CGS (CIGS) layers used as the input parameters for the simulations and physical models are found in [30, 14, 7].

The band gap energy of a semi-conductor plays an important role in the development and design of solar cells; it defines the absorption range of the cell, the amount of absorbed photons and the maximum achievable V_{oc} and J_{sc} [23]. When a solar cell is illuminated, only the photons having energy higher than the bandgap energy (E_g) of the semiconductor are absorbed and create electron hole pairs [16]. For the solar cells, the absorption range of solar spectrum is defined by [20]:

$$\lambda = \frac{1.24}{E_g(\text{eV})} \quad (1)$$

The temperature dependence of bandgap in semiconductors is described in literature [31, 32]. Using Varshni relation temperature dependence of the bandgap in semiconductors can be described as [33]:

$$E_g(\text{eV}) = \frac{E_{g0}{}^{-\alpha T^2}}{\beta + T} \quad (2)$$

where, $E_g(T)$ is the band gap of the semiconductor at some temperature T, which may be direct or indirect, $E_g(0)$ its value at $T \approx 0$ 0K and α and β are constants. The values of α and β for the semiconductor material CIGS in Table 1 [34], and E_{g0} for CGS and CIGSare 1.73 eV, 1.21 eV respectively.

The variation of band gap of CGS top-cell and CIGS bottom-cell for different temperatures ranging from 300-400 K is shown in the Fig. 2. From this figure, we notice that the gap energy decreases with increasing temperature for both materials.

The temperature affects the solar cells in different ways. It is well known that the physics governing solar cells operation is extremely temperature dependent. The materials parameters like the energy gap (E_g), mobilities (μ_n and μ_p), and carriers densities (N_c and N_v) are also temperature dependent. Furthermore, the absorbed energy that is not converted to electricity,is converted to heat and thus increases the temperature inside,the cells non-uniformly much beyond the ambient temperature.The used temperature dependenceformulas and the parameters for some semiconductor materials(CGS,CIGS) properties in the Table 1 [24, 35].

4. RESULTS AND DISCUSSIONS

4.1 Tandem Solar Cell Characteristics at 300 K

The performance of a CGS/CIGS tandem cell at the ambient temperature 300 K and for standard spectrum AM1.5G (100 mW/cm^2) was simulated and the cell was optimized [14]. The short-circuit current density matching between the top and the bottom cells, is obtained for an optimized value of 0.19 μm of the top CGS base layer [14]. The obtained results are given in Table 2.

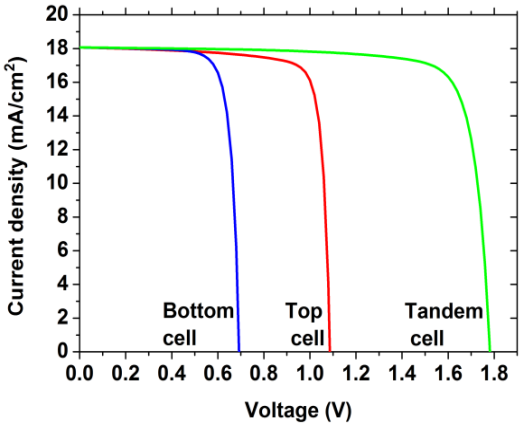

Fig. 2 – *J-V* characteristics for the CGS top-cell, CIGS bottom-cell and CGS/CIGS tandem cell under short-circuit current densities matching

4.2 Effect of Temperature on the Optimized (CGS/CIGS) Tandem Solar Cell

After optimized of the CGS/CIGS tandem solar cell, the effect of temperature on the CGS/CIGS tandem solar cell is investigate bed with two components: Top cell (CGS) and Bottom cell (CIGS). The operating temperature of the cells was varied from 300 to 400 K at intervals of 20 K. The simulation results are shown in Fig. 3. From these simulation results, we can see a small increase of the short current density with the operating temperature increases in both Fig. 3(a) Bottom (18.06-18.136 (mA/cm²)) and Fig. 3(b) Top (18.06-18.129 (mA/cm²)) and Fig. 3(c) tandem (18.06-18.133 (mA/cm²)) cells.

The variation is more important in the Bottom cell, because the Top cell is considered as a filter for the Bottom cell. This is due to the diminution of the energy gap E_g of the semiconductor. As shown the Fig. 2 (the absorption range of the bottom CIGS cell widens with the diminution of the gap of the CGS material constituting the top cell).

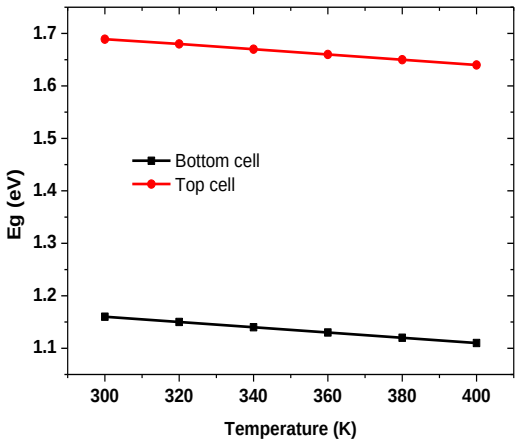

Fig. 3 – Variation of band gap of CGS top-cell and CIGS bottom-cell versus temperature

Table 1 – Dependence of material parameters on temperature

Parametres	Equation	CIGS/CGS
Band gap E_g (eV)	$E_g(\text{eV}) = \frac{E_{g0}^{-\alpha T^2}}{\beta + T}$	$1.21 - \frac{3.6E-4T^2}{350+T} / 1.73 - \frac{3.6E-4T^2}{350+T}$
Valence band effective density of states N_v (cm^{-3})	$N_v(T) = \left(\frac{T}{300}\right)^{3/2} NV300$	$3.46\times10^{15}(T)^{3/2}$
Conduction band effective density of states N_c (cm^{-3})	$Nc(T) = \left(\frac{T}{300}\right)^{3/2} NC300$	$4.24\times10^{14}(T)^{3/2}$
Electron mobility μ_n (cm²/V·s)	$\mu_{n0} = \left(\frac{T}{300}\right)^{-3/2} \mu_n$	$\mu_{n0} = 100\times\left(\frac{T}{300}\right)^{-3/2}$
Hole mobility μ_p (cm²/V·s)	$\mu_{p0}(T) = \left(\frac{T}{300}\right)^{-3/2} \mu_p$	$\mu_{p0}(T) = 25\times\left(\frac{T}{300}\right)^{-3/2}$

Table 2 – Optimized photovoltaic parameters of top, bottom and tandem solar cells under short-circuit current densities matching

	J_{sc}(mA/cm²)	V_{oc} (V)	FF (%)	η (%)
CGS Top-cell	18.06	1.08	82.88	16.26
CIGS Bottom-cell	18.06	0.7	79.46	9.93
CGS/CIGS Tandem cell	18.06	1.78	82.88	26.21

This is also due to the increase of the material conductivity because of the variation of the electron hole pairs mobility [23], as shown in expressions (3) and (4):

$$\sigma = q(\mu_n(T) + \mu_p(T))n_i(T), \quad (3)$$

$$J = \sigma\varepsilon. \quad (4)$$

Where σ is the material conductivity, n_i is intrinsic concentration, μ_n and μ_p are electrons and holes mobility, q is the elementary charge ε is electrical field intensity and J is the current density. These two phenomena accompanying the temperature increase allow the exploitation of more photons in the tandem cell. The increase in the short circuit current with temperature is about 0.005 mA/cm²/K.

The current density-voltage (J-V) characteristics of p-n junction solar cells under steady state illumination can most simply be described using single exponential model as, where, J_{ph} represents the photogenerated current density, V is the terminal voltage, voltage developed across the junction, k is the Boltzmann constant and n is the ideality factor [20].

$$J = -J_{ph} + J_0\left(e^{qV/nKT} - 1\right) \quad (5)$$

Due to the augmentation of the darkness current density J_0 (reverse saturation current density) of the cell, the opencircuit voltage decreases linearly with the increase of temperature. This is true for the top cell, bottom cell and the monolithic tandem cell.

The open-circuit voltage is the maximum voltage available from a solar cell. Eq. (5) at $J = 0$ yields the expression for V_{oc} as:

$$V_{oc} = \frac{nKT}{q} \ln\left(\frac{J_{sc}}{J_0(T)} + 1\right) \quad (6)$$

Where k is the Boltzmann's constant, T is the temperature, q is the charge of an electron and J_0 is the reverse saturation current density.

Where, $J_{sc} \approx J_{ph}$, V_{oc} is related to J_{sc} and J_0 and hence to E_g. For a high V_{oc}, a low J_0 is absolutely necessary.

While, the open circuit voltage decreases almost linearly with the increase of temperature in both Top (1.08-0.82 V) and Bottom (0.69-0.47 V) and tandem (1.78-1.3 V) cells.

It means that V_{oc} decreases almost linearly with increasing temperature. In (1), the reverse saturation current density J_0 is given by [36]

$$J_0 = q\left(\frac{D_n}{L_n N_A} + \frac{D_p}{L_p N_D}\right) n_i^2 \quad (7)$$

Where J_0 increases linearly with n_i^2 and

$$n_i^2(T) = N_c N_v exp - \left(\frac{E_g}{kT}\right) \quad (8)$$

In the foregoing equations, D_n, D_p, L_n, L_p are the electron and hole diffusion coefficients, diffusion lengths, respectively; N_A, N_D are the acceptor and the electron concentrations, respectively; and n_i^2 and E_g are the intrinsic carrier concentration and band gap. Where, N_c, N_v are effective density of states in conduction band, valance band respectively.

Combining Eqs. (7) and (8), the expression for J_0 can be written terms of temperature and bandgap energy [37,38] as:

$$J_0(T) = CT^3 \exp\left(\frac{-E_g}{kT}\right) \quad (9)$$

In the above equation, doping and the material parameters of solar cells are combined in this one constant C [38]. The important solar cell parameters for the model calculations are the temperature and bandgap. The higher the bandgap, lower will be the saturation current density.

According to (6), (7), and (8), it is seen that V_{oc} decreases with increasing T, due to the increase in n_i and the reduction of diffusion length (i.e., the increase in recombination).

Thedecrease in V_{oc} with increasing temperature arises mainly from $n_i\left(J_0 \infty n_i^2\right)$. Moreover, larger E_g will result in smaller n_i; thus, V_{oc} is more stable.

Fig. 4(a-d) show simulated photovoltaic parameters of the CGS, CIGS single solar cells and CGS/CIGS tandem solar cell as function of the temperature at 300 K to 400 K.

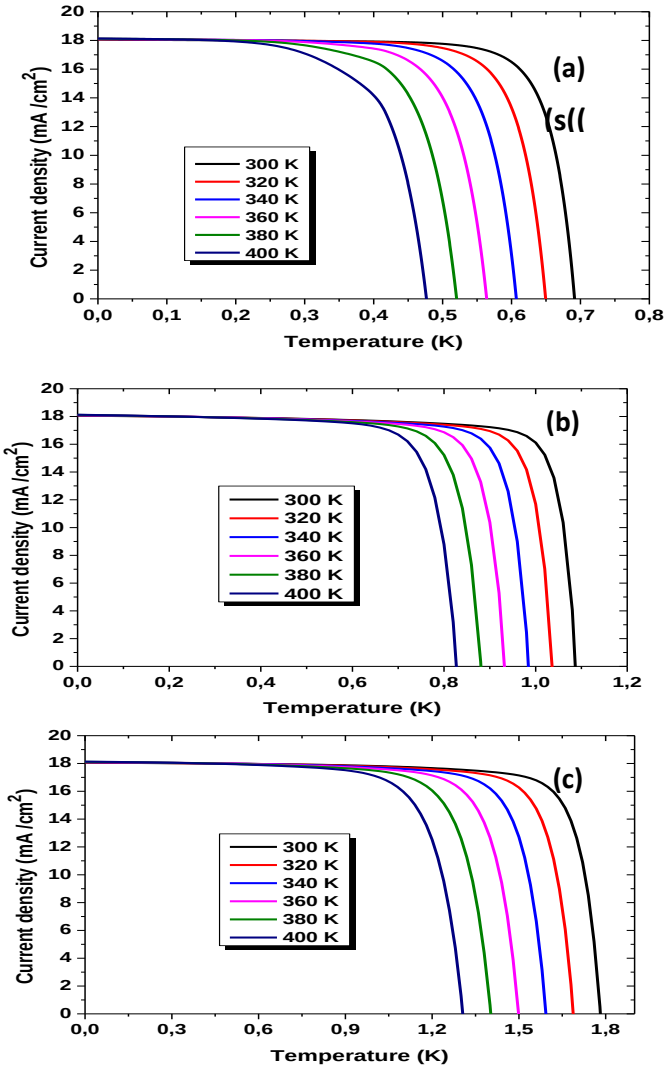

Fig. 4 – (J-V) characteristics for the (a) CIGS bottom-cell, CGS top-cell (b) and (c) CGS/CIGS tandem cell as function of the temperature

The short-circuit current density J_{sc} in Fig. 4(a) shows an increases with the increase in temperature in both cases. The variation in short circuit current density with temperature is primarily due to the change in bandgap with temperature [16] Generally, for most semiconductors, as the temperature increases, the bandgap decreases [16]. Consequently, the solar cell responds to longer wavelength regions in the solar spectrum and J_{sc} increases. Thus, J_{sc} is roughly proportional to the incident spectral intensity at wavelengths near the band edge [20].

The CGS, CIGS single solar cells and CGS/CIGS tandem solar cell as function of the temperature is shown in Fig. 4(b). It can be clearly observed that the open-circuit voltage (V_{oc}) decreases with the increase in temperature, whereas it increases with increasing bandgap, at 300 K V_{oc} value is (1.086, 0.692,1.78 V) and decreases further to (0.826, 0.47, 1.3 V) at 400 K for CGS, CIGS single solar cells and CGS/CIGS tandem solar cell respectively. The decrease in bandgap with increasing temperature results in lower V_{oc}.

In Fig. 4(c), is shown the variation of the tandem

cell *FF* with varying of the temperature.

Fill factor is determined with the decreases with increasing temperature, materials. The decrease in *FF* is mainly controlled by decrease in V_{oc} whereas increase in J_{sc} with temperature does not contribute much to *FF* [17].

In Fig. 4(d), is shown the change in efficiency with temperature for he CGS, CIGS single solar cells and CGS/CIGS tandem solar cell. The efficiency decreases further with increasingtemperature. The decrease in η with temperature is mainly controlled by the decrease of V_{oc} and *FF* with temperature.

In the Table 3 shows the temperature dependences of the CGS, CIGS single solar cells and CGS/CIGS tandem solar. Here, we use the relative temperature coefficient (*TC*) of cell parameters (V_{oc}, J_{sc}, *FF*, η) to compare the temperature dependences of different kinds of solar cell which is defined as [22]:

$$TC = \frac{1}{parameter(T = 300K)} \times \frac{d(parameter)}{dT} \times 100\% \quad (9)$$

The tandem cell operating temperature efficiency was found to be (– 0.34 %/K), we can see that our simulated results are in good agreement with simulation result in literature [39] which is slightly higher than that of CGS solar cell (– 0.29 %/K), but markedly better than that of CIGS solar cell (– 0.41 %/K). The single junction cell a base CIGS

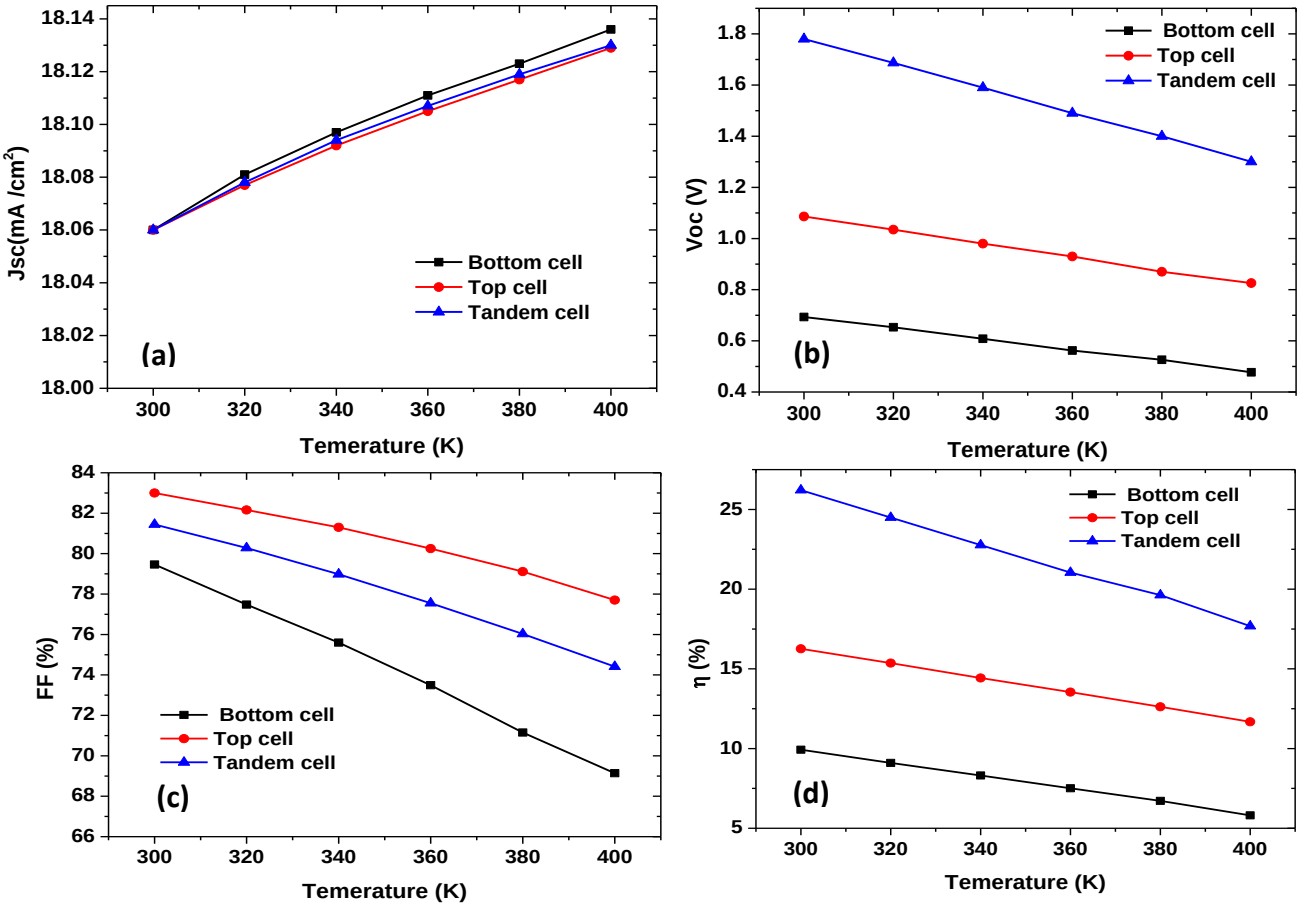

Fig. 4 – Simulated photovoltaic parameters of the CGS, CIGS single solar cells and CGS/CIGS tandem solar cell as function of the temperature

Table 3 – Calculated temperature dependences of CGS/CIGS tandem cell PV parameters compared with those of single-junction CGS and CIGS cells (*TC* = temperature coefficient)

Parameters / Type of cell		CGS	CIGS	CGS/CIGS
η at 300 K	η (%)	16.26	9.93	26.21
	$d\eta/dT$ (%/K)	–0.0477	–0.0414	–0.092
	TC (%/K)	–0.29	–0.41	–0.34

5. CONCLUSION

The temperature dependence of performance parameters (short-circuit current density J_{sc}, open-circuit voltage V_{oc}, fill factor *FF* and conversion efficiency η) of solar cells based on CIGS material has been investigated in the temperature range from 300 to 400 K. The maximum achievable, J_{sc}, V_{oc}, *FF* and η of solar cells, calculated for AM1.5G, are nearly the same as in the literature. With increasing temperature, the short-circuit current density of the CGS top-cell, the CIGS bottom-cell and the whole CGS/CIGS tandem cell increases. But, the open-circuit voltage, the fill factor and

the conversion efficiency of the CGS top-cell, the CIGS bottom-cell and the whole CGS/CIGS tandem cell decrease. The tandem cell operating temperature efficiency is found to be (– 0.34 %/K) which is slightly higher than that of the CGS solar cell (– 0.29 %/K), but it is better than that of the CIGS solar cell (– 0.41 %/K).

REFERENCES

1. K. Agrawal, V. Patil, G.T. Chavan, G. Yoon, J. Kim, J. Park, S. Pae, J. Kim, E.-C. Cho, J. Yi, *J. Mater. Sci. Mater. Electron.* **31**, 9826 (2020).
2. T.E. Taouririt, A. Meftah, N. Sengouga, M. Adaika, S. Chala, A. Meftah, *Nanoscale* **11**, 23459 (2019).
3. L. Ghalmi, S. Bensmaine, M. Elbar, S. Chala, H. Merzouk, *J. Nano- Electron. Phys.* **14** No 6, 06033 (2022).
4. F. Rasouli, M.R. Madani, *Opt. Quantum Electron.* **52**, 481 (2020).
5. S. Chala, M. Bdirina, M. Elbar, Y. Naoui, Y. Benbouzid, T.E. Taouririt, M. Labed, R. Boumaraf, A.F. Bouhdjar, N. Sengouga, F. Yakuphanoğlu, S. Rahmane, *Trans. Electr. Electron. Mater.* **23**, 544 (2022).
6. G.K. Gupta, A. Dixit, *Opt. Mater.* **82**, 11 (2018).
7. M. Elbar, S. Tobbeche, *Energy Procedia* **74**, 1220 (2015).
8. J. Madan, Shivani, R. Pandey, R. Sharma, *Sol. Energy* **197**, 212 (2020).
9. A.D. Adewoyin, M.A. Olopade, O.O. Oyebola, M.A. Chendo, *Optik* **176**, 132 (2019).
10. S. Chala, R. Boumaraf, A.F. Bouhdjar, M. Bdirina, M. Labed, T.E. Taouririt, M. Elbar, N. Sengouga, F. Yakuphanoğlu, S. Rahmane, Y. Naoui, Y. Benbouzid, *J. Nano- Electron. Phys.* **13** No 1, 01009 (2021).
11. M. Toghyani Rizi, M.H. Shahrokh Abadi, M. Ghaneii, *Optik* **155**, 121 (2018).
12. M.A. Shafi, L. Khan, S. Ullah, M.Y. Shafi, A. Bouich, H. Ullah, B. Mari, *Optik* **253**, 168568 (2022).
13. I. Gharibshahian, S. Sharbati, A.A. Orouji, *IET Optoelectron.* **14**, 199 (2020).
14. M. Elbar, S. Tobbeche, A. Merazga, *Sol. Energy* **122**, 104 (2015).
15. A. Soheili, M. Hayati, F. Shama, *Optik* **222**, 165461 (2020).
16. S.M. Sze, *Physics of Semiconductor Devices* (John Wiley & Sons: NewYork: 1981).
17. P. Singh, S.N. Singh, M. Lal, M. Husain, *Sol. Energy Mater. Sol. C.* **92**, 1611 (2008).
18. M. Jeng, Y. Lee, L. Chang, *J. Phys. D. Appl. Phys.* **42**, 105101 (2009).
19. Y. Da, Y. Xuan, *Sol. Energy* **115**, 109 (2015).
20. P. Singh, N.M. Ravindra, *Sol. Energy Mater. Sol. C.* **101**, 36 (2012).
21. J.C.C. Fan, *Sol. Cells* **17**, 309 (1986).
22. M. Yunaz, I.A. Sriprapha, K. Hiza, S. Yamada, A. Konagai, *Jpn. J. Appl. Phys.* **46**, 1398 (2007).
23. M. Abderrezek, M. Fathi, S. Mekhilef, F. Djahli, *Int. J. Renew. Energy Res.* **5**, 629 (2015).
24. *ATLAS, Version 5.20.2.R, SILVACO Int. St. Clara* CA, 2015. (2015).
25. S. Chala, N. Sengouga, F. Yakuphanoğlu, S. Rahmane, M. Bdirina, İ. Karteri, *Energy* **164**, 871 (2018).
26. M. Elbar, B. Alshehri, S. Tobbeche, E. Dogheche, *phys. status solidi (a)* **215**, 1700521 (2018).
27. S. Chala, N. Sengouga, F. Yakuphanoglu, *Vacuum* **120**, 81 (2015).
28. P. Jackson, D. Hariskos, E. Lotter, S. Paetel, R. Wuerz, R. Menner, W. Wischmann, M. Powalla, *Prog. Photovoltaics Res. Appl.* **19**, 894 (2011).
29. G.A. Landis, *Proc. Third World Conf. Photovolt. Energy Convers.* (2003).
30. S. Tobbeche, S. Kalache, M. Elbar, M.N. Kateb, M.R. Serdouk, *Opt. Quantum Electron.* **51**, 284 (2019).
31. P. Varshni, *Phys.* **34**, 149 (1967).
32. R. Passler, *phys. status solidi (b)* **216**, 975 (1999).
33. Tom Markvart, Luis Castafier, *Handbook of Photovoltaics: Section Finder* (Elsevier: 2003).
34. S.R. Kodigala, *Thin Films and Nanostructures* **35**, 505 (2010).
35. M.I. Hossain, A. Bousselham, F.H. Alharbi, *Mater. Technol.* **28**, No 1-2, 88 (2013).
36. X.-M. Cai, S.-W. Zeng, X. Li, J.-Y. Zhang, S. Lin, et al., *IEEE Trans. Electron Dev.* **58**, 3905 (2011).
37. Gerald Siefer, Andreas W. Bett, *Prog. Photovolt. Res. Appl.* **22**, 515 (2012).
38. M.E. Nell, A.B. Barnett, *IEEE Trans. Electron Dev.* **34** No 2, 257 (1987).
39. P. Chelvanathan, M.I. Hossain, N. Amin, *Curr. Appl. Phys.* **10**, S387 (2010).

ACKNOWLEDGEMENTS

M. Elbar et al. would like to thank the Laboratory of Metallic and Semiconducting Materials, University of Biskra, and the Algerian General Directorate of Scientific Research and Technological Development (DGRSDT) for their scientific and academic support.